Radiogenic and stable Ce isotope measurements by 1 thermal ionisation mass spectrometry

Pierre Bonnand, Claudine Israel, Maud Boyet, Régis Doucelance, Delphine Auclair

Radiogenic and stable Ce isotope measurements by thermal ionisation mass spectrometry

P. Bonnand[1*], C. Israel[1], M. Boyet[1], R. Doucelance[1], D. Auclair[1]

[1]Université Clermont Auvergne, CNRS, IRD, OPGC, Laboratoire Magmas et Volcans, F-63000 Clermont-Ferrand, France.

*Corresponding author

Email address: pierre.bonnand@uca.fr

Tel. No: +33 (0)473346783

Abstract

Techniques for the separation of Cerium (Ce) from silicate matrices and for the analysis of radiogenic (ε^{138}Ce) and mass dependent (δ^{142}Ce) Ce isotope variations by Thermal Ionisation Mass Spectrometer (TIMS) are presented in this study. We developed a static acquisition method associated with 10^{13} Ω amplifiers that allows (i) the precise determination of the ^{140}Ce peak tailing effect on the lighter Ce isotopes, and (ii) the reduction of the counting time necessary to obtain high precision isotopic composition. The long-term reproducibility obtained for our Ce reference material (Ce-LMV) on the ^{138}Ce/^{142}Ce ratio is 0.02257053 ± 0.00000061 (27 ppm, 2 s.d., n = 48). The new Ce-LMV has been calibrated against the commonly used AMES reference material (0.02257426 ± 0.00000068 (30 ppm, 2 s.d., n = 25). The static cup configuration also allows a more stable determination of the tailing effect from the ^{140}Ce isotope peak onto ^{136}Ce and ^{138}Ce. Finally, the 10^{13} Ω amplifiers permit a better determination of the tailing effect during low voltages measurements. A new method to measure mass dependent Ce isotope variations based on the double spike method has also been developed. Uncertainty propagation calculations demonstrate that the best spike mixture is a ^{136}Ce-^{138}Ce-^{140}Ce triple spike. We have calibrated an in-house triple spike used to correct for instrumental mass bias effect and fractionation of Ce isotopes during Ce separation. Numerical simulations demonstrate the effect of potential isobaric interferences from Ba, Nd and La and highlight the need for an efficient chemical separation. Two loading techniques were tested for triple spike measurements (oxide and metal). The best reproducibility for δ^{142}Ce is obtained for the metal runs and is about ± 0.028 ‰. Although this technique has been developed for silicate matrices, the mass spectrometry method can be applied to other matrices such as carbonates. The newly calibrated Ce reference material is available to the community upon request.

1. Introduction

The Rare Earth Elements (REE) are a group of 17 elements (Lanthanides (La to Lu) as well as Scandium and Yttrium), widely used in the geosciences community because of their similar behaviour in natural systems. REE can be found as minor or trace elements in most natural environments and are sometimes more concentrated in some minerals (e.g. monazite) or CeO_2 nanoparticles. The main characteristic of the REE group is that their oxidation state in most natural system is REE^{3+} except for Ce and Eu. Europium can form Eu(II) ions in reduced conditions and Ce is more stable in Ce(IV) in oxidised conditions. The differences in chemical behaviour between Ce and Eu compared with the rest of the REE have been extensively used in the literature via the positive and negative anomalies. For example, seawater is characterised by a large negative Ce anomaly due to the insolubility of Ce(IV) relative to other REE(III).[1] In this case, Ce is oxidised to Ce(IV) and is removed from seawater leaving the residue Ce depleted and therefore creating a negative Ce anomaly. Cerium anomalies have also been used in high temperature settings such as zircon crystallisation.[2-5] Indeed, the amplitude of the Ce anomaly in zircon is directly proportional to the redox conditions and can potentially be used as an oxybarometer.[2,3] Cerium is a lithophile element and behaves incompatibly in magmatic systems, meaning that upon melting and/or crystallisation Ce remains in the melt.

Cerium has four stable isotopes, ^{136}Ce, ^{138}Ce, ^{140}Ce and ^{142}Ce with relative abundance of 0.185 %, 0.251 %, 88.45 % and 11.114 %, respectively (Fig. 1)[6]. Cerium isotopes vary in relative abundance by two orders of magnitude, which makes analyses more challenging than, for example, Nd, which only vary by a factor of five. Indeed, ^{138}Ce and ^{136}Ce are about 400 times less abundant than the main Ce isotope (^{140}Ce). The small Ce isotopic variations observed in natural systems mean that high precision measurements are required. Furthermore, ^{138}Ce is affected by isobaric interferences from ^{138}Ba, which is the most abundant Ba isotope, and from ^{138}La, which is the least abundant La isotope. There is also an isobaric interference from ^{142}Nd onto ^{142}Ce. Additionally, ^{136}Ce and ^{138}Ce are affected during measurement on a TIMS by tailing effect from mass ^{140}Ce.[7] The measurement of Ce isotopes at high

77 precision is thus challenging. This requires both a good chemical separation between Ce and the
78 isobaric interference elements (mainly Ba and Nd) and a specific analytical setting.

79 Cerium isotopes have been previously studied for the radiogenic variations of ^{138}Ce.[8-14] The La-Ce
80 systematic is based on the β-decay of ^{138}La to stable ^{138}Ce. The low abundance of ^{138}La and its long
81 half-life (β-decay; $t^{1/2}$ = 292.5 x 10^9 years, 14) means that the observed variations in ^{138}Ce/^{142}Ce are
82 small (~80-120 ppm) compared to variations in the Sm-Nd systematic (~600 ppm).[16] Nevertheless, the
83 La-Ce system has been successfully applied as a geochemical tracer together with other isotopic
84 systems (Rb-Sr, Sm-Nd, Lu-Hf, Re-Os and U-Th-Pb) and for the age determination of rocks.[17-21] It has
85 also been successfully used for terrestrial and lunar basalts, manganese nodules and seawater.[22-26]
86 The Ce isotopes variations can be reported in different notations.[12] In this study, we choose to report
87 the variations in three notations:

88 $$^{138}Ce/^{142}Ce_{sample} \quad (1)$$

89 which is the tail, oxide and mass fractionated corrected ratio (see text below for details).

90 $$^{138}Ce/^{136}Ce = \frac{^{138}Ce/^{142}Ce}{^{136}Ce/^{142}Ce_{natural}} \quad (2)$$

91 where the ratio ^{136}Ce/^{142}Ce$_{natural}$ is fixed to 0.01688.[23]

92 $$\varepsilon^{138}Ce = (\frac{^{138}Ce/^{142}Ce_{sample}}{^{138}Ce/^{142}Ce_{LMV}} - 1) * 10000 \quad (3)$$

93 where ^{138}Ce/^{142}Ce$_{LMV}$ is the ratio obtained for our Ames Ce reference material (Ce-LMV).

94 Mass dependent Ce isotopic variations have also been recently explored.[27] Due to the chemical
95 behaviour of Ce described above, it has been suggested that Ce isotopes could be used as a redox
96 proxy.[28] Mass dependent Ce isotope measurements have been performed for natural Fe-oxides and
97 absorption experiments.[29] The results suggest that Ce isotopes are fractionated during absorption

98 onto Fe-oxyhydroxides and that isotopic fractionation occurring in natural systems could be linked to
99 redox reactions. More recently, CeO_2 nanoparticles have also been analysed in order to characterise
100 their impact on natural systems.[30] Several studies have presented analytical techniques to separate
101 and analyse mass dependent Ce isotope variations.[27,30] In these studies, mass dependent Ce isotope
102 variations have been analysed with Multi-Collector Inductively Coupled Plasma Mass spectrometers
103 (MC-ICPMS) using the external doping technique with either Sm[26] or Ba.[30] The Ce isotopic composition
104 is reported as the per mil variation from the Ce isotope reference material LMV using the equation:

105 $$\delta^{142}Ce = \left(\frac{^{142}Ce/^{140}Ce_{sample}}{^{142}Ce/^{140}Ce_{LMV}} - 1 \right) * 1000 \quad (4)$$

106 In this study, we propose a new methodology to measure radiogenic variations of Ce isotopes. We
107 developed a new static cup configuration on a Thermal Ionisation Mass Spectrometer (TIMS) that
108 allows the simultaneous measurement of Ce isotopes (and its isobaric interference elements) together
109 with four masses used to define the tailing from ^{140}Ce onto ^{136}Ce and ^{138}Ce. In comparison to previous
110 techniques that used a multi-static acquisition method (2 to 6 lines), this new method allows the
111 reduction of the length of high precision measurements. We also present a new triple spike (^{136}Ce-
112 ^{138}Ce-^{140}Ce) method to measure mass dependent Ce isotope variations with a better precision than
113 previous analytical methodologies.

114 **2. Analytical techniques**

115 **2.1. Chemical separation**

116 Reference materials and samples were prepared in the clean laboratory in class 100 laminar flow
117 hoods at the Laboratoire Magmas et Volcans (Clermont Ferrand). All acids (HCl, HNO_3 and HF) were
118 distilled in the Savillex® acid still DST-1000. PFA Savillex® beakers were cleaned with concentrated
119 HNO_3 and HCl on the hotplate at 115 ºC and then rinsed in ultrapure H_2O. Our high purity Ce metal
120 reference material was bought from AMES Laboratory and will be thereafter called Ce-LMV. M.
121 Willbold provided the second reference material analysed in this study (Ce-AMES; 6). The Ce reference

material (Ce-LMV) was dissolved in HCl on the hotplate for 48 hours. Approximately 50 mg of whole rock basalts reference materials (BHVO-2 and BCR-2) were dissolved using concentrated HNO_3-HF-HCl acid mixtures. The fully dissolved sample was evaporated to dryness and then re-dissolved in 2.5 M HCl for chemical separation.

The chemical separation method used in this study is modified after Tazoe et al. (2007)[31], Li et al. (2015)[32] and Bellot et al. (2015)[20]. Only a brief description is given here. The chemical separation developed to separate the Ce fraction to silicate matrices involved three columns. The first step was used to separate the REEs from the main cations of the matrix (Fig. 2). In order to achieve this separation, the samples were loaded in 2.5N HCl onto 1 mL of AG50 X8, 200-400 mesh resin in Bio-Rad 10 ml column. Prior to the chemistry, the resin was cleaned with 10 ml 6M HCl. The REE stuck to the resin while the main cations were eluted from the resin. Ba was then eluted in 2M HNO_3 and the REE were finally eluted in 6M HCl (Fig. 2a). The second column procedure was designed to separate Ce^{4+} from the other REE using LnSpec Eichrom resin (50-100 µm) in 2 ml Bio-Rad columns.[31] The oxidation of Ce from Ce^{3+} to Ce^{4+} was achieved with 0.5ml of $NaBrO_3$ (20mM) in 10M HNO_3. Prior to the chemistry, the resin was cleaned with 5 ml 6M HCl. The samples were loaded onto 0.1 mL LnSpec Eichrom resin in 10M HNO_3 + $NaBrO_3$ and Ce^{4+} stuck to the resin while the remaining REE^{3+} were eluted in the loading solution (Fig. 2b). The Ce fraction was eluted in 6M HCl + H_2O_2. Finally, the samples were then processed through the first step of the chemistry to make sure the Ce fraction was cleaned of any remaining matrix cations.

2.2. Mass spectrometry

Isotopic measurements were performed on a ThermoScientific Thermal Ionisation Mass spectrometer Triton Plus (TIMS) at the Laboratoire Magmas et Volcans. The Ce reference materials were analysed in both oxide and metal forms using the double filament technique. For the oxides analyses, the Ce fraction was loaded in HCl onto outgassed Re filament together with 0.5 µL of 1 M H_3PO_4. For the metal runs, the Ce fraction was loaded in HCl onto outgassed C-doped zone refined Re

147 filaments. Aquadag was added to outgassed Re filament and the filament was then re-degassed. The
148 carbon acted as a reducer and stopped the emission and ionisation of Ce oxides. During a typical Ce
149 metal measurement the CeO/Ce ratio was always lower than 0.002.

150 During the course of this study, several cup configurations have been tested (Table 1). Firstly, the
151 Ce-AMES reference material was analysed using the dynamic method previously proposed to measure
152 Ce isotopes.[7,20] This cup configuration requires a multi-static acquisition method. The first line is for
153 measuring Ce, Nd, La and Ba masses with $^{139}La^{16}O$ in the central cup (Table 1). The tailing is measured
154 on the second line after a -0.5 mass unit (MU) jump. In this configuration, both elemental and tailing
155 signals are measured using 10^{11} Ω resistors. For this study, we have established a new cup
156 configuration where mass and half-mass signals are measured simultaneously. In this case, the
157 acquisition is achieved in a static mode and different resistors can be used for both signals and tailing
158 masses. This technique has two main advantages. First, the tailing effect on mass ^{136}Ce and ^{138}Ce can
159 be estimated more precisely. Second, the static acquisition method reduces the duration of our
160 isotopic measurements by a third.

161 The oxide runs were performed in two main cup settings (Table 1). In the first setting (cup
162 configurations #2 and 3), $^{140}Ce^{16}O$ was not measured and the signal was adjusted to have 10 V (0.1 nA)
163 of $^{142}Ce^{16}O$. In the second setting (cup configuration #4, 5 and 6), $^{140}Ce^{16}O$ was measured in H2. The
164 difference between cup configurations in each setting is the amplifier combination (Table 1). The cup
165 configuration #7 was designed to measure all Ce isotopes and isobaric interferences together with
166 tailing masses. Due to the increased amount of ^{136}Ce and ^{138}Ce after spike addition, the 10^{11} Ω and 10^{13}
167 Ω amplifiers were used for all elemental signals and tailing masses, respectively. The cup configuration
168 #8 was designed to measure Ce and its isobaric interference isotopes in metal form. In this setting, all
169 cups were associated with 10^{11} Ω amplifiers and no tailing masses were monitored. Typical runs on
170 the mass spectrometer consist of 27 blocks of 20 cycles with 8.462 seconds integration time. Each
171 block started with a baseline measurement of 30 seconds. The gain calibrations for the 10^{10}, 10^{11} and

10^{12} Ω resistors were performed daily using the ThermoScientific software built in gain routine (at 3.33 V). The gain calibrations for the 10^{13} Ω resistors were performed weekly (when used) with Nd signals following the ThermoScientific procedure.

2.3. The triple spike technique

The use of an isotopically enriched solution ("double spike") to correct for fractionation of stable isotopes during sample processing and for instrumental mass bias effects has long been recognised as a powerful tool.[33-35] This methodology has now been successfully applied to many isotopes systems including Fe, Sr, Zn, Cd and Cr.[36-39] For Ce, the double spike technique is applicable to both terrestrial and extra-terrestrial samples because the Ce isotope radiogenic and nucleosynthetic variations are small and will not generate a large influence in the spike deconvolution. Moreover, this technique allows the determination of Ce concentration by isotope dilution.

In this study, we explore the best spike composition to measure mass dependent Ce isotopic variations. Three spikes are commercially available: ^{136}Ce-^{140}Ce, ^{138}Ce-^{140}Ce and ^{142}Ce. The ^{142}Ce spike has already been used for isotope dilution measurement in previous studies. In order to optimise carefully the spike composition, a number of mixtures between commercially available spikes have been investigated (Table 2). This requires: (1) establishing the most appropriate spike composition; (2) solving the double spike equations and (3) adding the appropriate amount of spike to the reference material. The optimisation is described by the uncertainty magnification term, γ:

$$\gamma = \sigma_{DS}/\sigma_{nat}, \quad (5)$$

where σ_{DS} is the uncertainty obtained from the double spike deconvolution procedure and σ_{nat} is the uncertainty of the natural unspiked run. Our calculations are similar to those described by Galer (1999)[40] but we deconvolve the runs using the exponential mass fractionation law. The spike compositions used in the calculations are given in Table 2 and the results of the calculations are presented in Figure 3. Three spike mixtures were investigated: ^{136}Ce-^{140}Ce-^{142}Ce, ^{138}Ce-^{140}Ce-^{142}Ce and ^{136}Ce-^{138}Ce-^{140}Ce. In Figure 3, the lower uncertainty magnification term is obtained for the ^{136}Ce-^{138}Ce-

197 ^{140}Ce triple spike. The best proportion of ^{136}Ce-^{140}Ce spike in the triple spike mixture is about 50 %. In
198 order to calculate the optimal spike/sample ratio, the deconvolution program is run using different
199 proportions of spike and sample. We use an ion model based on the one described by Ludwig (1986)[41]
200 to calculate the uncertainty on signal intensity of each isotope which is then propagated to calculate
201 the uncertainty on the double spike deconvolution procedure. The uncertainty magnification term is
202 calculated using Monte Carlo simulation in which the uncertainties of the four Ce isotopes signals are
203 used to generate 540 data points for each analysis. These points have a Gaussian distribution around
204 the mean value. The results obtained after the Monte Carlo simulations (540 cycles) are processed
205 through the deconvolution procedure and the uncertainty (σ_{DS}) of the deconvolved data is calculated.
206 For the triple spike ^{136}Ce-^{138}Ce-^{140}Ce, the uncertainty magnification term is always less than 4. Figure
207 3b illustrates the optimal spike/sample ratio for the two double spikes (^{136}Ce-^{140}Ce and ^{138}Ce-^{140}Ce)
208 and the triple spike (^{136}Ce-^{138}Ce-^{140}Ce). It is important to note that the two double spikes can produce
209 low uncertainty magnification terms but the proportion of spike required is high (spike/sample ratio
210 = 0.8). The triple spike however has a more flatten uncertainty model curve, which means that not
211 only the uncertainty magnification term is better for almost all mixtures but also that optimal spiking
212 is facilitated. The best spike/sample ratio for the triple spike is 0.33.

213 An in-house ^{136}Ce-^{138}Ce-^{140}Ce triple spike was prepared from ^{136}Ce-^{140}Ce and ^{138}Ce-^{140}Ce cerium
214 oxides spikes purchased from IsoFlex® and their enrichment factors were 42.5 % and 41.6 %,
215 respectively. Two double-spike solutions were made by dissolving the Ce-oxides in 6M HCl-H_2O_2. The
216 Ce spikes were purchased in oxide form and H_2O_2 helped to reduce Ce and facilitated the dissolution.
217 The triple spike was then prepared by mixing the double spikes in the appropriate proportions. The
218 triple spike was calibrated by TIMS at the Laboratoire Magmas et Volcans using the loading techniques
219 described above. The pure Ce-LMV reference material, the pure triple spike and spike/standard
220 mixtures were analysed. The isotopic composition of the triple spike is then calculated by treating the
221 pure triple spike as an unknown. The composition of the triple spike was derived from 26 separate
222 analyses and is reported in Table 3.

3. Data Processing

The Ce isotopic composition of the samples and reference materials was determined offline but baseline and gain corrections were performed online with the ThermoScientific software. The deconvolution procedures used for unspiked and spiked runs are described in details in the paragraphs below. The deconvolution procedure for both unspiked and spiked runs can be divided in three main steps: tail correction on mass ^{136}Ce and ^{138}Ce, oxide corrections and mass bias fractionation corrections.

3.1. Tail correction

The large dynamic range in Ce isotopes, with ^{140}Ce accounting for 88.45% of total Ce, has long been recognised as a problem for obtaining high precision Ce isotope measurements (e.g. 7). Indeed, the small proportion of ^{136}Ce and ^{138}Ce, 0.19 and 0.25% respectively, means that we need to measure high intensity beams (e.g. 80 V (0.8 nA) for $^{140}Ce^{16}O$) in order to obtain accurate and precise Ce isotopic compositions. It has been shown that running at high intensities produces a tailing effect on mass ^{136}Ce and ^{138}Ce. Classically, the tailing contribution was calculated with half masses analysis (e.g. 7) in a dynamic sequence (cup configuration #1, Table 1). In this contribution, we developed a simultaneous measurement of the Ce isotopes and of the tailing contribution. Two cups were intercalated between masses 152 and 154 and one cup between 154 and 156 (see Table 1, Fig. 4). This new cup configuration allows the measurement of intensities generated by the large ^{140}Ce beam on mass 156.5 and 154.6. The intercalated cup positions were determined by measuring the distance between the cups on large mass scans using a stable Ce beam. This step is critical in order to perform an accurate tail correction. In order to determine the contribution of the tailing on mass ^{136}Ce and ^{138}Ce, we fitted an exponential equation through the measured masses. The increased integration time (from 4s to 8s) compared to our dynamic measurements means that the tailing contribution can be assessed more precisely. Furthermore, the static run suppresses the need for magnet shift and allows a more stable measurement. The uncertainty induced by small offset in magnet position described in details in Willig

and Stracke (2017)[13] can therefore be avoided. The static cup configuration allows a more stable determination of the tail effect (0.6 to 0.9 ε unit) compared to previous studies (0.0 to 1.6 ε unit[42] and 0.15 to 1.8 ε unit[13]). All ^{136}Ce and ^{138}Ce signals mentioned hereafter in the manuscript are tail corrected (unless noted otherwise).

3.2. Oxide correction and mass bias correction

During the measurement of Ce isotopes in oxide form, the measured raw signals are the sums of the isotopes of interest and an oxide interference following the equation:

$$^{X}Ce^{16}O = I^{(X+16)} - {}^{(X-2)}Ce^{18}O \quad (6)$$

where X can be 138, 140 and 142 and $I^{(X+16)}$ is the measured intensities on the mass X+16 corresponding to the three oxide masses. With R = ^{18}O/^{16}O, equation 6 can be easily expressed as:

$$^{X}Ce^{16}O = I^{(X+16)} - {}^{(X-2)}Ce^{16}O * R \quad (7)$$

The oxide correction methodology used in this study follows a similar protocol to that of Willig and Stracke (2017)[13] although it is adapted for the triple spike deconvolution procedure.

For the unspiked runs, an iterative process was followed whereby the ratio R is assumed to be 0.00213 and signals measured on masses 154, 156 and 158 are corrected for the contribution of ^{136}Ce^{18}O, ^{138}Ce^{18}O and ^{140}Ce^{18}O respectively following equation 7. The ^{138}Ce/^{142}Ce and ^{140}Ce/^{142}Ce ratios (when measured) were corrected for mass bias fractionation using the exponential law and the ^{136}Ce/^{142}Ce ratio of 0.01688.[43-45] Using the obtained Ce isotopes intensities the fractionation factor (β) is then determined using the exponential mass fractionation law:

$$\beta = \frac{\ln\left(\frac{^{136}Ce/^{142}Ce_{true}}{^{136}Ce/^{142}Ce_{measured}}\right)}{\ln\left(\frac{M^{136}Ce^{16}O}{M^{142}Ce^{16}O}\right)} \quad (8)$$

where $^{136}Ce/^{142}Ce_{measured}$ is the tail and oxide corrected $^{136}Ce^{16}O/^{142}Ce^{16}O$ measured ratio and $^{136}Ce/^{142}Ce_{true}$ is fixed to 0.01688. $M^{136}Ce^{16}O$ and $M^{142}Ce^{16}O$ are the atomic masses of $^{136}Ce^{16}O$ and $^{142}Ce^{16}O$, respectively. Using the fractionation factor calculated above, a new R value can be calculated using the equation:

$$R = \frac{\frac{^{136}Ce^{16}O}{^{142}Ce^{18}O}_{measured}}{\frac{^{136}Ce}{^{142}Ce}_{true}} * \left(\frac{M^{136}Ce^{16}O}{M^{142}Ce^{18}O}\right)^{\beta} \quad (9)$$

where $^{136}Ce^{16}O/^{142}Ce^{18}O_{measured}$ is the measured ratio. The new R value is then used to calculate new oxide contributions on masses 152, 154 and 156. This iterative deconvolution is conducted until the R value reaches a plateau which is usually obtained after three iterations. The β value obtained on the last iterative step is used to calculate the corrected Ce isotopic composition. When $^{140}Ce^{16}O$ is not measured, a fixed value for the $^{140}Ce/^{142}Ce$ ratio is used to correct the contribution of $^{140}Ce^{18}O$ on $^{142}Ce^{16}O$ signals.

For the triple spiked analysis, we follow the same principle except that mass bias fractionation is solved following the equation 10:

$$F^i\left(P_{sp}^{ref}, f_{nat}, f_{mix}\right) = P_{sp}^{ref} r_{sp}^i + (1 - P_{sp}^{ref}) r_{nat}^i \left(\frac{M^i}{M^{ref}}\right)^{f_{nat}} - r_{mix}^i \left(\frac{M^i}{M^{ref}}\right)^{f_{mix}} = 0 \quad (10)$$

where r^i_{sp} is the isotope ratio of i in the spike, r^i_{nat} and r^i_{mix} are the measured isotope ratios of i in the sample and mixture, and M_i and M_{ref} are the true masses of the isotope oxides (i+16). The F^i function is a closure function for the spike sample mixture, which must be equal to zero. The equation is solved using an iterative Newton-Raphson procedure that recovers the proportion of spike in the mixture (P^{ref}_{sp}), the fractionation factor for the spike-sample mixture (f_{mix}) and finally the fractionation factor for the sample (f_{nat}). Using the measured $^{136}Ce^{16}O/^{142}Ce^{18}O$ ratio and the mixture fractionation factor (f_{mix}), we calculated a new R value which is then used to correct for oxide interferences. The deconvolution procedure finishes when R value does not change, within 5 ppm, from one iteration

290 step to the other. We then obtain our final f_{nat} value that is used to calculate the isotopic composition
291 of the original sample. The isotope ratios for the Ce-LMV reference material used for referencing our
292 isotope data (to calculate $\delta^{142}Ce$) in this study were obtained by TIMS by internal normalisation to
293 $^{136}Ce/^{142}Ce$ ratio as described above and was recalculated in the ^{140}Ce space (i.e. ^{140}Ce as a
294 denominator). This yielded $^{136}Ce/^{140}Ce = 0.00212$, $^{138}Ce/^{140}Ce = 0.0248$ and $^{142}Ce/^{140}Ce = 0.12588$.

295 For triple spike runs performed in metal form, the same procedure was used with metal Ce
296 intensities except that no tailing and oxide corrections were performed (see below for details).

297 **4. Results and Discussion**

298 **4.1. Separation of Ce from the samples matrix**

299 High precision measurements of Ce isotopes by TIMS require the separation of Ce from the sample
300 matrix in order to minimise isobaric interferences. Several methods have previously been reported to
301 separate Ce from silicate matrices. The main problem with obtaining high precision Ce isotopes
302 measurement, especially in metal mode (see below), is the complete removal of Ba during the
303 chromatography procedure. The efficacy of our Ce separation technique was tested using synthetic
304 multi-elemental solution and a certified basalt reference material (BHVO-2). Figure 2 shows well-
305 defined and separated elution peaks during the chromatography procedure. Importantly, interfering
306 elements such as Ba and Nd are separated from Ce in the first and second step of the column
307 chemistry, respectively. After the three steps column procedure, the Ba/Ce and Nd/Ce ratios are
308 decreased to 0.002 and 0.001 respectively. The total blank of our Ce separation procedure is about
309 0.5 ng, which is negligible (<0.1%) compared to the amount of Ce processed through the columns
310 (~700 ng).

311 **4.2. Accuracy and reproducibility of radiogenic measurements**

312 Two Ce reference materials were analysed during the course of this study for their radiogenic Ce
313 isotope composition. The results obtained in the different analytical setups are summarised in Table
314 4 and Figure 5. Wilbold (2007)[7] demonstrated that Ce isotope measurements in metal form were

315 strongly affected by Ba interference most likely coming from the filaments. We therefore decided to
316 measure radiogenic Ce isotope in oxide form only, testing several cup configurations. Using the multi-
317 static cup configuration, the $^{138}Ce/^{142}Ce$ obtained for the Ce_{AMES} reference material is 0.0225743 ±
318 0.0000005 (2 s.d., n = 5). For the static cup configuration without $^{140}Ce^{16}O$, the $^{138}Ce/^{142}Ce$ obtained
319 for the Ce_{AMES} and Ce_{LMV} reference materials are 0.0225743 ± 0.0000007 (2 s.d., n = 25) and 0.0225705±
320 0.0000006 (2 s.d., n = 48) respectively. Finally, for the static cup configuration with $^{140}Ce^{16}O$, the
321 $^{138}Ce/^{142}Ce$ obtained for the Ce_{AMES} and Ce_{LMV} reference materials are 0.0225746 ± 0.0000001 (2 s.d.,
322 n = 5) and 0.0225706 ± 0.0000005 (2 s.d., n = 7) respectively. The $^{138}Ce/^{142}Ce$ ratios obtained for both
323 Ce reference materials in all cup configurations are always identical within uncertainty (Table 4). There
324 is also a good agreement between our data and the literature values but our reproducibility is better
325 than previously reported.[6,12,18-20] Contrary to earlier studies, the data presented here have not been
326 normalised to a reference session which tends to improve the external reproducibility. In the cup
327 configurations #4, 5 and 6, the $^{140}Ce/^{142}Ce$ ratios were also determined and we obtained for our
328 reference materials $^{140}Ce/^{142}Ce_{AMES}$ = 7.94416 ± 0.00023 (2 s.d., n = 5) and $^{140}Ce/^{142}Ce_{LMV}$ = 7.94397 ±
329 0.00018 (2 s.d., n = 7). There is about 100 ppm difference between our value and the value reported
330 by Willig and Stracke (2017)[13]. The difference between these values is possibly due to the use of two
331 different mass spectrometers with variable faraday cups ages[46] and/or due to the different cup
332 configurations (^{140}Ce measured in axial and L1 cups). However, this small difference is negligible for
333 the correction of the contribution of $^{140}Ce^{18}O$ onto $^{142}Ce^{16}O$ when $^{140}Ce^{16}O$ is not measured. Two
334 geological reference materials (BHVO-2 and BCR-2) were also analysed for their Ce radiogenic isotopic
335 compositions. The $^{138}Ce/^{142}Ce$ ratios together with the $^{140}Ce/^{142}Ce$ ratios are given in Table 1. For
336 BHVO-2, the $^{138}Ce/^{142}Ce$ and $^{140}Ce/^{142}Ce$ ratios obtained are 0.0225650 ± 0.0000004 (2 s.d., n = 2) and
337 7.94389 ± 0.00003 (2 s.e., n = 1), respectively. For BCR-2, the $^{138}Ce/^{142}Ce$ and $^{140}Ce/^{142}Ce$ ratios
338 obtained are 0.0225670 ± 0.0000005 (2 s.d., n = 5) and 7.94362 ± 0.00003 (2 s.e., n=1), respectively.
339 The $^{138}Ce/^{142}Ce$ values presented in this study are in agreement with previous estimates of the
340 $^{138}Ce/^{142}Ce$ ratios for these two geological reference materials.[13,19,20]

As described above, several cup configurations were tested during the course of this study. Each of those has advantages and inconveniences and we will now try to compare the results with previously published results and highlight the gain of the new technique. In terms of reproducibility, the $^{138}Ce/^{142}Ce$ ratio can be measured, using the static cup configuration, at about 25 ppm, which is comparable to the reproducibility obtained for the same reference material during dynamic measurements. However, the run duration is divided by 1.5 and the amount of Ce required also decreases to 700 ng. The main advantage of the method used in this study is the ability to reduce the counting time by 30% to obtain similar internal reproducibility. If the Ce quantity is the same, the signal intensity can be increased and then the internal precision will be better since the counting statistic is the main factor limiting the internal precision. We also performed Ce isotopic measurements with 250 ng of Ce and we could run CeO at about 2.5V (0.025 nA) of $^{142}Ce^{16}O$. The reproducibility obtained is about 45 ppm, which is slightly higher than the optimised conditions but still acceptable for many applications. Compared to literature values, our reproducibility is similar or better than recently published Ce isotopes measurements (Table 1).[13] The second advantage of the simultaneous measurement of Ce isotopes and the half masses tailing is that it does not require mass shift during the run. Finally, the main inconvenience of using our new cup configuration is the correction for Ba interference on the ^{136}Ce and ^{138}Ce isotopes. The static cup configuration uses the less abundant ^{134}Ba (~2.4 %) whereas the multi-static method used the slightly more abundant ^{137}Ba (~11.2 %). This reduces our ability to measure small amount of Ba by about 4 which could potentially be a problem. However, the chemical separation presented in this study is designed to effectively separate Ba from the Ce fraction to level well below detection limit. Furthermore, due to the high ionization potential of BaO[47] and the likely presence of Ba phosphate, running in oxide mode reduces the amount of emitted Ba, which means that the proposed method enables high precision Ce isotopes measurements.

4.3. The utility of 10^{13} amplifiers

366 In previous studies, the faraday cups were always coupled with 10^{11} Ω amplifiers and this
367 configuration allows the definition of the tailing from $^{140}Ce^{16}O$ when routine beams of 10 V (0.1 nA) of
368 $^{142}Ce^{16}O$ were measured. One of the aims of this study is to develop a new method to measure Ce
369 isotopes at high precision with smaller quantities. To this end, we used 10^{13} Ω resistors on the tailing
370 masses. The signal/noise on the 10^{13} Ω resistors is supposed to be 10 times better than the typical 10^{11}
371 Ω resistors. Thus the new amplifiers allow the measurements of small beams with better precision
372 than typical 10^{11} Ω amplifiers. In Figure 6, the intensities measured for the tailing masse 154.5 with
373 two different resistors are shown. The signal measured (0.35 fA) with 10^{13} Ω resistor is less noisy by a
374 factor of five compared to 10^{11} Ω resistor which is comparable to the predicted improvement of ten.
375 The standard deviation for a stable beam of 0.35 fA improves from 0.35 fA when using 10^{11} Ω amplifier
376 and 4 seconds integration time to 0.25 fA (10^{11} Ω amplifier and 8s integration time) and 0.05 fA (10^{13}
377 Ω amplifier and 8s integration time). For runs at high intensities (0.1 nA $^{142}Ce^{16}O$), the tailing measured
378 with 10^{11} Ω resistors is precisely defined (Fig. 4). As expected, the tailing produced during a low
379 intensity Ce isotope measurements (0.03 nA on $^{142}Ce^{16}O$) is much smaller than at high intensity
380 although its relative intensity compared to the measured Ce signals is the same (Fig. 4). Using 10^{13} Ω
381 resistors, we could define a good tailing where it was more difficult with typical 10^{11} Ω resistors. This
382 indicates that it is possible to produce high precision Ce isotopes measurements with lower signals
383 than previously suggested and 250ng Ce (~0.03 nA of $^{142}Ce^{16}O$) is enough to obtain a precise
384 $^{138}Ce/^{140}Ce$ ratio. We also performed a few experiments with ^{136}Ce and ^{138}Ce signals with 10^{13} Ω
385 resistors using the multi-static cup configuration (#1). The slow response time of these resistors means
386 that after the jump, it was not possible for the signals to go back to the baseline values in a reasonable
387 time. We therefore think that it is currently difficult to use 10^{13} Ω resistors in dynamic measurements.
388 The best cup configurations (#4 and #5, Table 1) for radiogenic Ce isotopic measurements are a
389 combination of 10^{10}, 10^{11}, 10^{12} and 10^{13} Ω resistors. If analysed, the main Ce peak ($^{140}Ce^{16}O$) is
390 measured with a 10^{10} or 10^{11} Ω resistor in high and low intensity runs, respectively. The second most
391 abundant Ce mass ($^{142}Ce^{16}O$) is always measured with 10^{11} Ω resistor. The low intensities signals on

masses $^{136}Ce^{16}O$ and $^{138}Ce^{16}O$ are measured using 10^{12} Ω resistors. Finally, the tailing masses in cups L4, L2, L1 and H1 are measured with 10^{13} Ω resistors. The best cup configuration used for the triple spike runs is a combination of 10^{11} and 10^{13} Ω resistors. The Ce masses and the tailing are measured with 10^{11} and 10^{13} Ω resistors, respectively.

The newly developed cup configuration allowed the determination of the tailing effect on masses ^{136}Ce and ^{138}Ce. The lack of jump and the longer integration time of the static measurement mean that the tailing is more stable. The long-term tailing correction for the data presented in this study is 0.73 ± 0.13 ε which is slightly better than the reproducibility obtained per session using the multi-static cup configuration #1 (from 0.14 to 0.51).[42] The tailing effect during analysis at low intensity (3 V $^{142}Ce^{16}O$) is similar (0.71 ± 0.15 ε unit) in size. This indicates that the newly developed cup configuration allows a more reproducible determination of the tailing effect from $^{140}Ce^{16}O$ onto masses $^{136}Ce^{16}O$ and $^{138}Ce^{16}O$.

4.4. Spike calibrations and mass dependent Ce isotope measurements

The triple spike was calibrated in oxide mode and the results are presented in Table 5 and Figure 7. Three spike mixtures were analysed and the $\delta^{142}Ce$ values recovered by the triple spike technique are within uncertainty of 0 ‰ as expected but the overall average value is slightly positive with $\delta^{142}Ce$ values ranging from -0.015 to 0.023 ‰. The best reproducibility is obtained by the spike/standard mixture ratio of 0.30 and is $\delta^{142}Ce$ = 0.023 ± 0.052 ‰ (2 s.d., n = 13). However, there is no difference between the three spike-sample mixtures analysed in this study. The internal uncertainty (2 s.e.) of measurements of $\delta^{142}Ce$ in the standard-spike mixture runs is usually better than 0.015‰. The results were deconvolved with and without tail correction. In this case, the tail correction does not change the deconvolved value suggesting that the increase in intensities due to spike addition is sufficient to make the contribution of tailing on masses 154 and 156 negligible. The large difference between our internal uncertainty and our external reproducibility is difficult to understand. One possibility is that

this difference originates from the oxide correction applied to the raw data. Further tests are needed to understand this observation.

A standard-spike mixture was also analysed in metal mode. In this case, no tailing correction was performed because of the increase in signal intensities with the spike addition. The main difference with the oxide run is the presence of small amount of Ba. The Ba interference correction is important during analysis in metal form. The cup configuration allows the measurement together with the Ce isotopes of ^{137}Ba that is slightly higher than ^{134}Ba. The Ba signals are difficult to control during TIMS measurements and are unpredictable. Several factors seem to favour Ba emission. Among them are a rapid heating and a high ionisation current. However, when the Ba interference is well controlled, the reproducibility obtained on the standard-spike mixture is δ^{142}Ce = -0.083 ± 0.028‰, which is better than the reproducibility obtained in oxide mode and in the methods proposed in the literature.[22,25] This value is slightly lighter than the expected δ^{142}Ce value of 0. The main reason for this discrepancy is probably the fact that the correction procedure is different between metal and oxide analyses.

4.5. Effects of isobaric interferences

In most natural samples, Ce is present as a trace element and Ba and Nd can be present as a minor component (Ba/Ce and Nd/Ce ratios up to 200 and 30, respectively). In some rare cases such as monazite, both Ce and Nd can be present at the percent level. The Ce separation is designed to remove the matrix elements and the main isobaric interference elements but it is nevertheless important to carefully consider the potential effects of isobaric interferences from Ba on ^{136}Ce and ^{138}Ce and Nd on ^{142}Ce. In order to correct for isobaric interferences in both unspiked and spiked runs, two key assumptions are made. Firstly, the instrumental mass bias for Ce, Ba and Nd is assumed to be the same for all elements involved. Secondly, the interfering elements are considered to have natural isotopic compositions because it is not possible to determine simultaneously the Ce, Ba and Nd isotopic compositions. It is well documented that cation exchange chromatography can lead to large isotopic

fractionation. The chemical separation is designed to remove the isobaric interference and the small quantities remaining in the Ce fraction is likely to be heavily fractionated.

In order to test the sensitivity of our interference corrections in the spike deconvolution procedure, we have performed some simple numerical calculations. A spiked Ce-LMV solution is "contaminated" with variable amounts of Ba, Nd and La, which have their isotopic compositions that differ from the "natural" composition by -3 ‰ to +3 ‰. These mixtures are then fractionated using the exponential mass fractionation law by the typical amount of TIMS Ce measurement. The resulting compositions are then put through our triple spike deconvolution procedure, which calculates the isotopic composition of the Ce-LMV reference material. These calculations are performed in metal form and the results are presented in Figure 8. The deconvolution procedure recovers a δ^{142}Ce of 0 when the natural compositions are assumed for Ba, Nd and La, as would be expected. However, it is important to note that the recovered δ^{142}Ce values deviate from zero when non-natural values are assumed. For example, if the contaminant Ba has an isotopic composition that is fractionated from the natural composition by 1 ‰ and the ^{137}Ba/^{142}Ce = 0.006, then the recovered δ^{142}Ce value is +0.1 ‰ (Fig. 8). This non-negligible interference correction should be applied with care. The chemical separation allows a good separation between Ce and its isobaric interferences. Typical silicate samples analysed in this study, after column chemistry, have ^{138}Ba/^{138}Ce, ^{143}Nd/^{142}Ce and ^{139}La/^{138}Ce ratios of less than 0.004, 0.0001 and 0.002 respectively. The uncertainty introduced by the interference correction would be negligible even in the case of non-natural isotopic composition of the contaminants.

5. Conclusions

A method has been developed that allows effective separation of small quantities of Ce (~700 ng) from silicate samples using a three-step column chemistry procedure. This chemical separation procedure allows the effective separation of Ce from Nd and Ba, two isobaric interference elements.

During the course of this study, several cup configurations were tested in order to measure radiogenic Ce isotopes at high precision. The newly developed static acquisition method allows the simultaneous measurement of the four Ce isotopes and their isobaric interferences (^{134}Ba, ^{139}La and ^{143}Nd) together with intercalated masses for tailing correction. The reproducibility obtained with two Ce reference materials (Ce-LMV and Ce-AMES) is about 27 ppm which is similar to previous TIMS methodologies. The main advantage of our new configuration is the reduced counting time necessary to obtain high precision data. This also indicates that high precision measurements can be performed with smaller amount of Ce ($\sim$ 700 ng). The use of the 10^{13} Ω resistors to measure the tailing masses allows the measurements of even smaller Ce quantities ($\sim$250ng) with a reproducibility of about 43 ppm. The new analytical technique allows a more stable determination of the tailing effect on masses ^{136}Ce and ^{138}Ce.

A triple spike method has been developed to measure mass dependent Ce isotopic variations. To this end, uncertainty models were calculated on three commercially available Ce spikes and the best mixture is a triple spike containing ^{136}Ce-^{138}Ce-^{140}Ce isotopes. The spike/standard ratio of 0.33 produces the best spiking mixture in order to reduce the uncertainty magnification produced by adding spike to the natural samples. Two analytical methods were used to measure stable Ce isotopes on the TIMS and the runs in metal produce the best reproducibility. The main problem with Ce isotopes measurements in metal is the correction for Ba interferences on ^{136}Ce and ^{138}Ce. However, the chemical separation described in this study allows an effective separation of Ba and Ce. We have also performed a number of calculations to characterise the sensitivity of our method to the interferences correction and the fact that we always assume natural compositions for the interfering elements. These calculations show that a small change in the isotopic composition will have a big impact on the recovered δ^{142}Ce values. It is therefore fundamental to perfectly isolate Ce from the matrix and the isobaric interference elements in order to produce accurate and precise mass dependent stable Ce isotope measurements.

References

1 H. Elderfield and M. J. Greaves, Nature, 1982, **296**, 214–219.

2 A. D. Burnham and A. J. Berry, Geochim. Cosmochim. Acta, 2012, **95**, 196-212.

3 D. Trail, E. B. Watson and N. D. Tailby, Nature, 2011, **480**, 79-82.

4 D. J. Smythe and J. M. Brenan, Earth Planet. Sci. Lett., 2016, **453**, 260–266.

5 D. J. Smythe and J. M. Brenan, Geochim. Cosmochim. Acta, 2015, **170**, 173-187.

6 K.J.R. Rosman and P.D.P. Taylor, Pure Appl. Chem., 1998, **70**, 217-236.

7 M. Willbold, J. Anal. At. Spectrom., 2007, **22**, 1364–1372.

8 T. Tanaka and A. Masuda, Nature, 1982, **300**, 515–518.

9 T. Tanaka, H. Shimizu, Y. Kawata and A. Masuda, Nature, 1987, **327**, 113–117.

10 P. Dickin, Nature, 1987, **325**, 337–338.

11 H. Shimizu, T. Tanaka and A. Masuda, Nature, 1984, **307**, 251–252.

12 H. Shimizu, H. Sawatari, Y. Kawata, P. N. Dunkley and A. Masuda, Contrib. Mineral. Petrol., 1992, **110**, 242–252.

13 M. Willig and A. Stracke, Chem. Geol., 2017, **476**, 119-129.

14 C. Schnabel, C. Münker and E. Strub, J. Anal. At. Spectrom., 2017, **32**, 2360-2370.

15 M. Tanimizu, Phys. Rev. C, 2000, **62**, 017601-1–017601-4.

16 S.-G. Lee, Y. Asahara, T. Tanaka, N. H. Kim, K. H. Kim, K. Yi, A. Masuda, Y. S. Song, Chem. Geol., 2010, **276**, 3-4, 360-373.

17 H. Shimizu, S. Nakai, S. Tasaki, A. Masuda, D. Bridgwater, A. P. Nutman and H. Baadsgaard, Earth Planet. Sci. Lett., 1988, **91**, 159-169.

18 S. Nakai, H. Shimizu and A. Masuda, Nature, 1986, **320**, 433–435.

19 R. Doucelance, N. Bellot, M. Boyet, T. Hammouda, C. Bosq, Earth Planet. Sci. Lett., 2014, **407**, 175–186.

20 N. Bellot, M. Boyet, R. Doucelance, C. Pin, C. Chauvel and D. Auclair, Geochim. Cosmochim. Acta, 2015, **168**, 261-279.

21 N. Bellot, M. Boyet, R. Doucelance, P. Bonnand, I. P. Savov, T. Plank, T. Elliott, Chem. Geol., 2018, https://doi.org/10.1016/j.chemgeo.2018.09.006

22 M. Tanimizu and T. Tanaka, Geochim. Cosmochim. Acta, 2002, **66**, 4007–4014.

23 A. Makishima and A. Masuda, Chem. Geol., 1994, **118**, 1–8.

24 H. Amakawa, J. Ingri, A. Masuda and H. Shimizu, Earth Planet. Sci. Lett., 1991, **105**, 554–565.

25 H. Shimizu, K. Tachikawa, A. Masuda and Y. Nozaki, Geochim. Cosmochim. Acta, 1994, **58**, 323–333.

26 H. Tazoe, H. Obata and T. Gamo, Geochem. Geophys. Geosyst., 2011, **12**, 1–14.

27 R. Nakada, Y. Takahashi and M. Tanimizu, Geochim. Cosmochim. Acta, 2013, **103**, 49-62.

28 R. Nakada, M. Tanaka, M. Tanimizu and Y. Takahashi, Geochim. Cosmochim. Acta, 2017, **218**, 273-290.

29 R. Nakada, Y. Takahashi and M. Tanimizu, Geochim. Cosmochim. Acta, 2016, **181**, 89-100.

30 A. Laycock, B. Coles, K. Kreissig and M. Rehkämper, J. Anal. At. Spectrom., 2016, **31**, 297-302

31 H. Tazoe, H. Obata and T. Gamo, J. Anal. At. Spectrom., 2007, **22**, 616–622.

32 C.-F. Li, X.-C. Wang, Y.-L. Li, Z.-Y. Chu, J.-H. Guo and X.-H. Li, J. Anal. At. Spectrom., 2015, **30**, 895-902.

33 M. H. Dodson, J. Sci. Instrum., 1963, **40**, 289–295.

34 F. Albarede and B. L. Beard, Rev. Mineral. Geochem., 2004, **55**, 113–152.

35 J. F. Rudge, B. C. Reynolds and B. Bourdon, Chem. Geol., 2009, **265**, 420–431.

36 M.-A. Millet, J. A. Baker and C. E. Payne, Chem. Geol., 2012, **304-305**, 18-25.

37 B. L. A. Charlier, I. J. Parkinson, K. W. Burton, M. M. Grady, C. J. N. Wilson and E. G. C. Smith, Geochim. Persp. Let., 2017, **4**, 35-40.

38 T. M. Conway, A. D. Rosenberg, J. F. Adkins and S. G. John, Analytica Chimica Acta, 2013, **793**, 44-52.

39 P. Bonnand, I. J. Parkinson, R. H. James, A.-M. Karjalainen and M. A. Fehr, J. Anal. At. Spectrom. 2011, **26**, 528–535.

40 S. J. G. Galer, Chem. Geol., 1999, **157**, 255–274.

41 K. R. Ludwig, U.S. Geol. Surv. Bull., 1986, **1622**, 219–221.

42 N. Bellot, PhD thesis, Universite Blaise Pascal, 2016.

43 H. Shimizu, N. Umemoto, A. Masuda and P. W. U. Appel, Geochim. Cosmochim. Acta, 1990, **54**, 1147–1154.

44 A. Makishima and E. Nakamura, chem. Geol., 1991, **94**, 1–11.

45 A. Makishima, H. Shimizu and A. Masuda, Mass Spectrosc., 1987, **35**, 64–72.

46 M. Garçon, M. Boyet, R. W. Carlson, M. F. Horan, D. Auclair and T. D. Mock, Chem. Geol., 2018, **476**, 493-514.

47 D. R. Lide, CRC Handbook of Chemistry and Physics, 1994, 75th ed. CRC Press.

Conflicts of interest

There are no conflicts to declare.

Acknowledgments

We would like to thank Matthias Willbold for providing his Ce reference material (Ce-AMES). PB would like to thank Alex Halliday for giving him the spikes. The reference material Ce-LMV is available upon request. We would like to thank Hauke Vollstaedt and Claudie Black for helpful discussions. We would like to thank Ryan Ickert for his thorough review that has improved the quality of this manuscript. This project has received funding from the European Research Council (ERC) under the European Union's Horizon 2020 research and innovation programme (Grant Agreement No 682778 - ISOREE). This is Laboratory of Excellence ClerVolc contribution number XXX.

Figures:

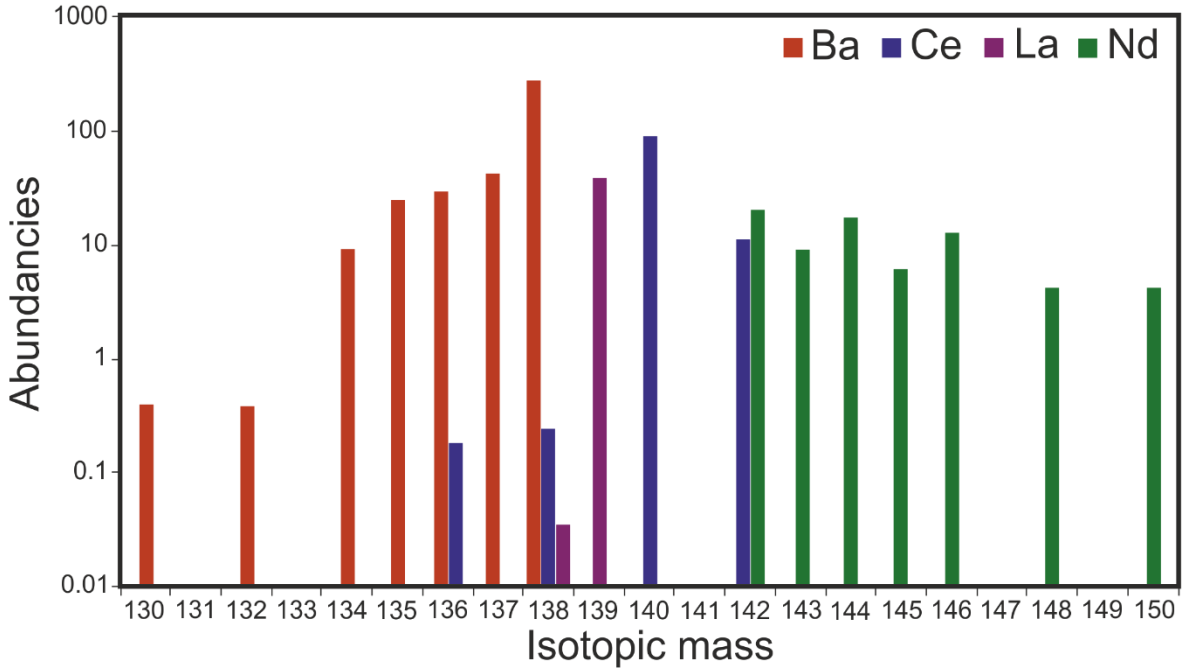

Figure 1: Ce, Nd, La and Ba isotopes abundances normalised to the primitive mantle elemental abundances.[48] Note the logarithmic scale.

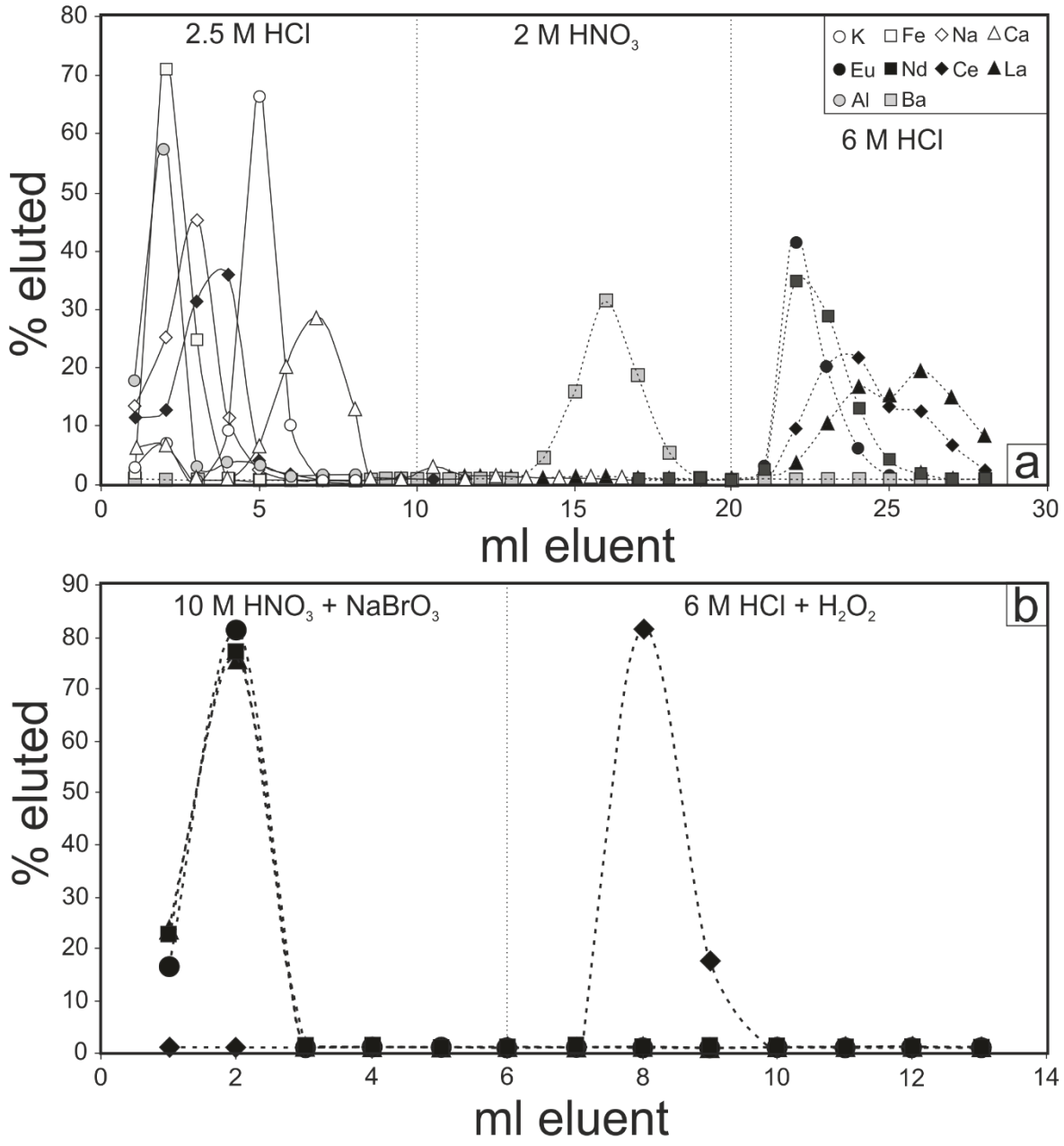

Figure 2: Elution curves for the first (a) and second (b) steps of the purification protocol used in this study. The first step was performed using AG50 X8, 200-400 mesh in 10 ml Bio-Rad columns. The second step was performed using using LnSpec Eichrom resin (50-100 µm) in 2 ml Bio-Rad columns.

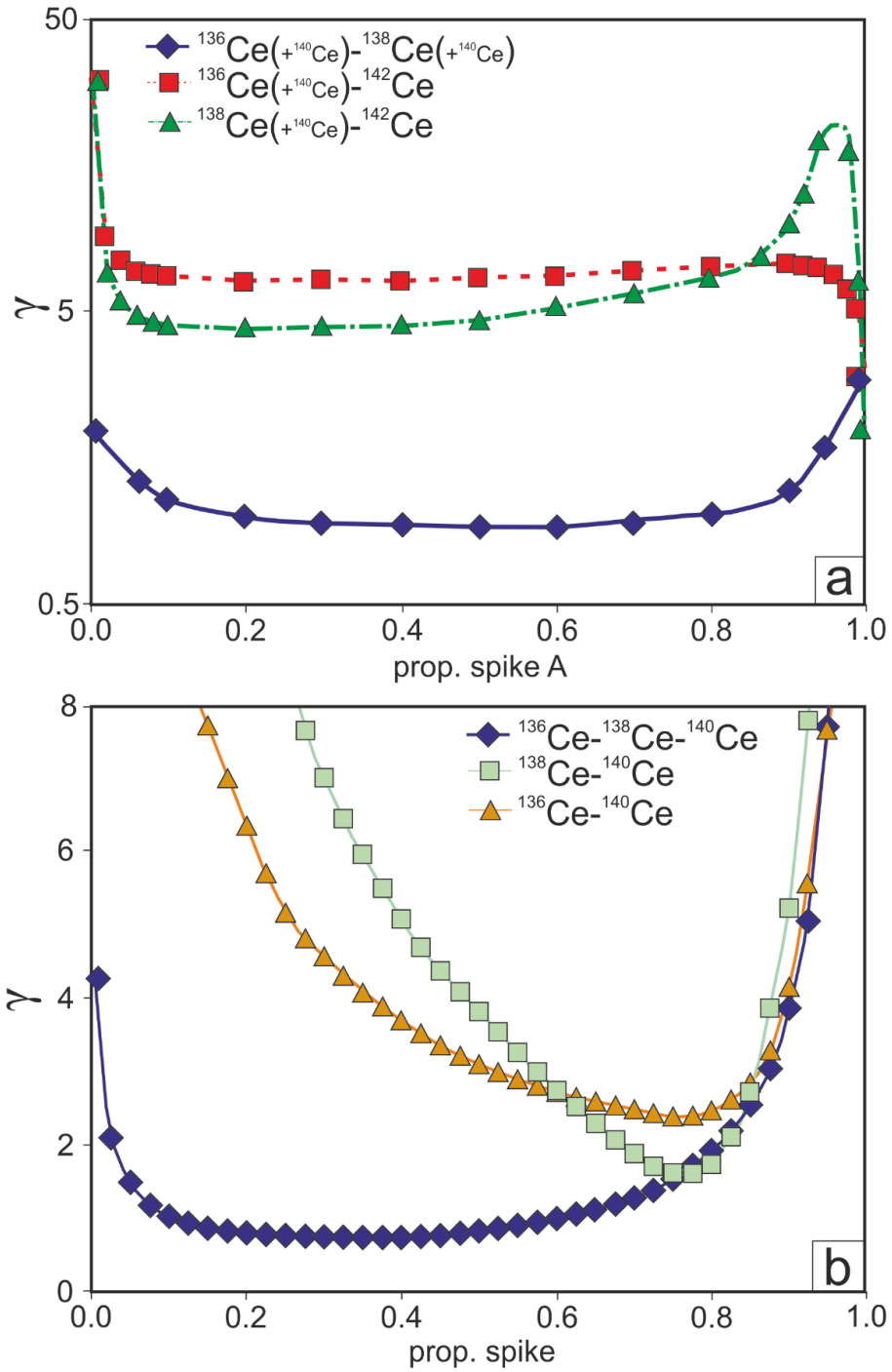

665

666 Figure 3: (a) Uncertainty magnification term (γ) for the deconvolved ^{142}Ce/^{140}Ce ratio as a function of
667 the proportion of spike A in the spike mixtures. The spike A is the first spike in the legend (for
668 example spike A is ^{136}Ce in the spike mixture ^{136}Ce-^{142}Ce). (b) Uncertainty magnification term (γ) for
669 three spikes (commercially available ^{136}Ce and ^{138}Ce spikes and a 50-50% mixing on these two same
670 spikes) versus the proportion of spike in the standard spike mixtures (see text for details). A lower
671 gamma (γ) value indicate a better spike mixture (a) or a better proportion of spike (b).

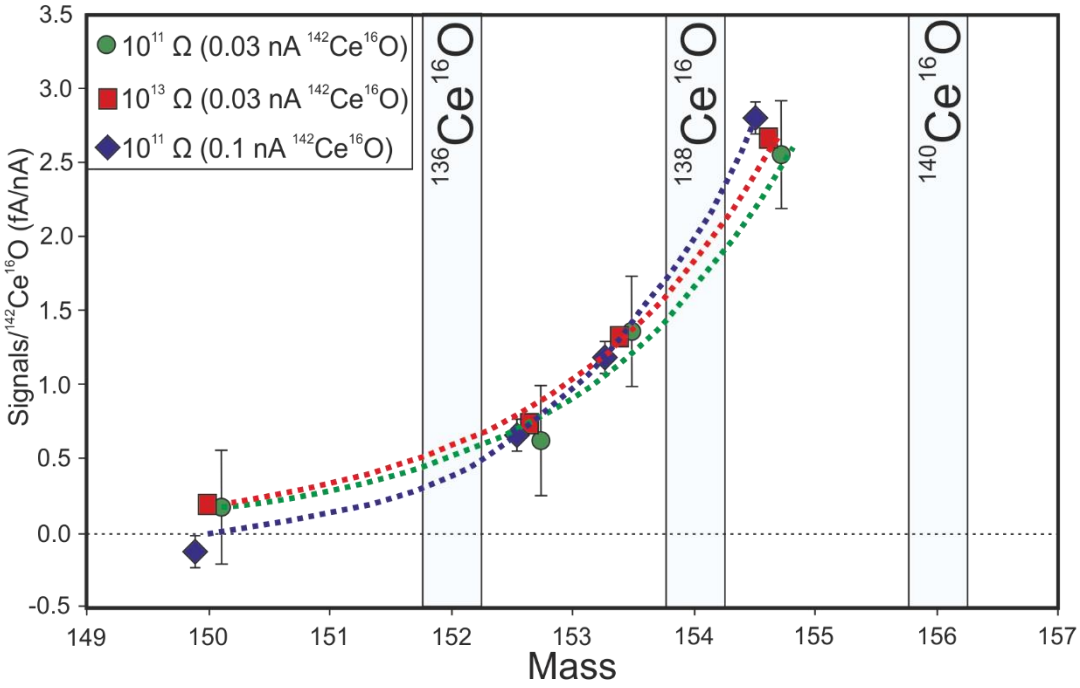

672

673 Figure 4: Tailing measured in three analytical settings: green is the tailing with high intensities using
674 10^{11} Ω resistor, blue is the tailing measured at low intensities using 10^{11} Ω resistors and red is the
675 tailing measured at low intensities using 10^{13} Ω resistors (See text for details). The measured
676 intensities (fA) on the tailing masses were divided by the intensities measured on $^{142}Ce^{16}O$ for each
677 runs (~0.03 nA for green and red and ~0.1 nA for blue). All tailing masses were measured on the same
678 masses but for a better visibility of the tailing on the figure, the green and blue points are artificially
679 moved by +0.1 and -0.1 mass unit respectively.

680

681

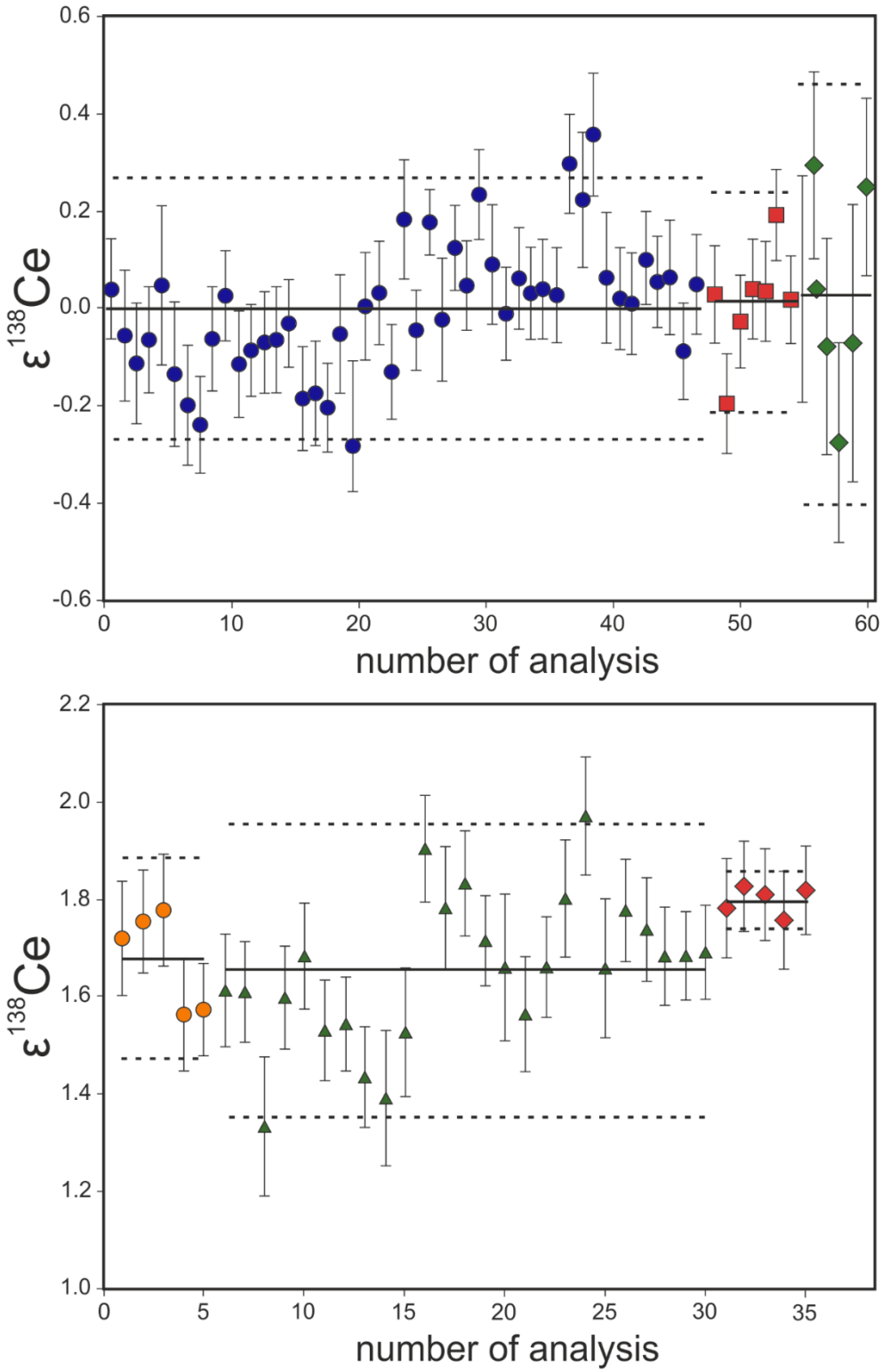

682

683 Figure 5: Long-term reproducibility of ε^{138}Ce for the LMV-Ce (a) and AMES-Ce (b) reference
684 materials. (a) The blue circles, red squares and green diamonds data were obtained with cup
685 configurations #3, #4 and #5. The green diamonds were run at lower intensities. (b) The orange
686 circles, green triangles and red diamonds data were obtained with cup configurations #1, #2 and #4.
687 The solid and dashed lines are the mean and 2 s.d. values for each configuration used in this study.

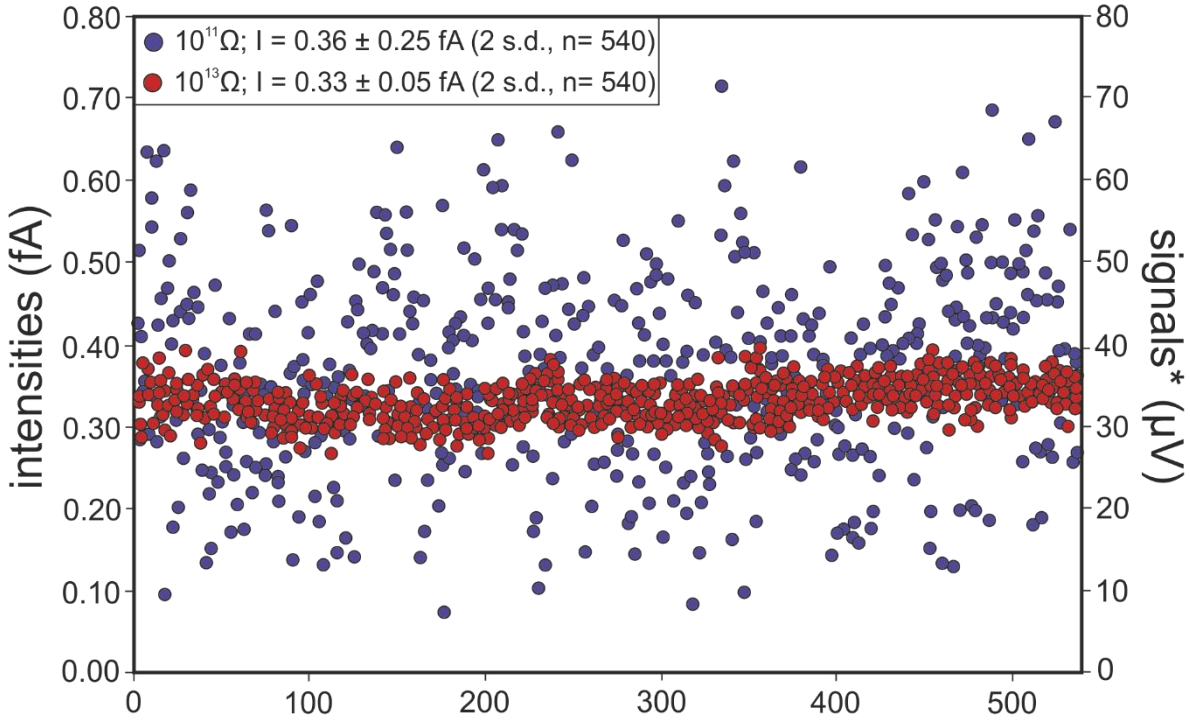

688

689 Figure 6: Typical signals measured at the tailing mass 154.5 with 10^{11} Ω (blue) and 10^{13} Ω (red)
690 amplifiers during two measurements performed with 0.1 nA on $^{142}Ce^{16}O$. The signals expressed in
691 voltages have been calculated relative to 10^{11} amplifiers.

692

693

694

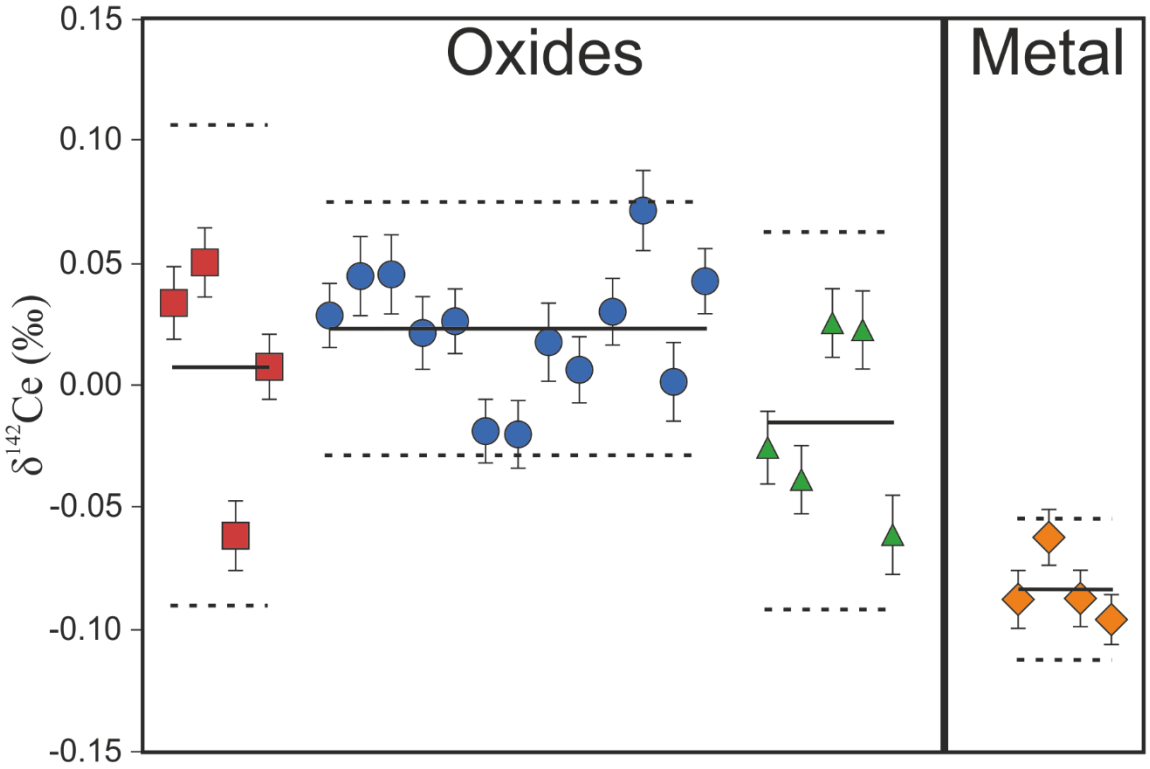

Figure 7: Mass dependent Ce isotopic compositions (δ^{142}Ce) for the Ce-LMV reference material. The squares, circles and triangles data points are three standard-spike mixtures run in oxides mode. The orange diamonds are one standard-spike mixture run in metal mode (see text for details). The error bars are internal uncertainties for each run. The solid and dashed lines are the mean and 2 s.d. values for the four standard-spike mixtures, respectively.

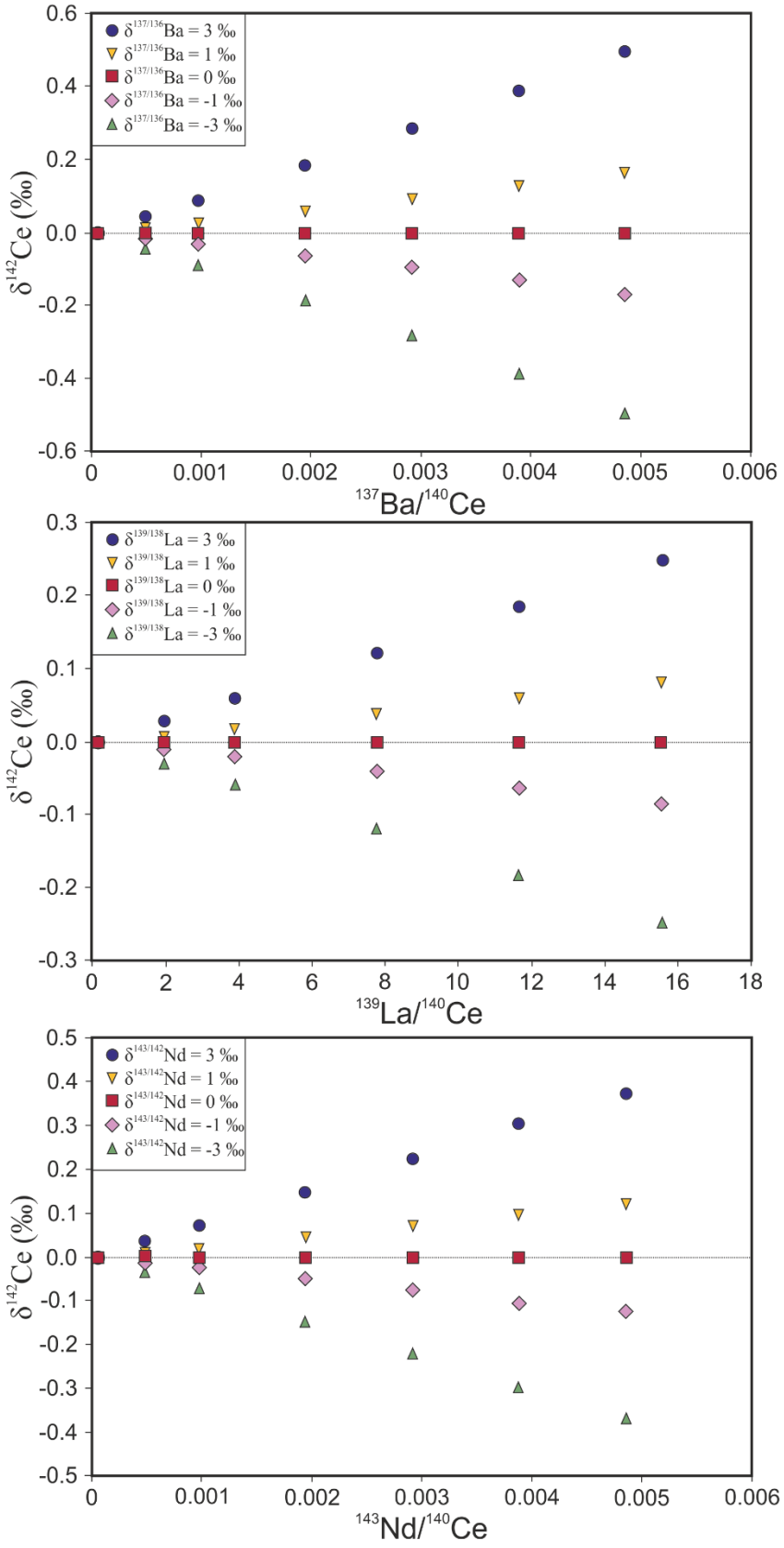

Figure 8: Effects of "non-natural" isobaric interferences from (a) Barium, (b) Lanthanum and (c) Neodymium on $\delta^{142}Ce$ as a function of the element/Ce ratio. The changing isotopic compositions for the interfering elements are shown by the different symbols.

706 Tables

707 Table 1: Cup configurations used on the Thermo-Scientific Triton plus TIMS at the Laboratoire Magmas et Volcans during the course of this study. The main
708 isotope masses are in bold; the interference masses are in italic. $^{134}Ba^{16}O$ is also ^{150}Sm and ^{150}Nd. $^{142}Ce^{18}O$ is also $^{143}Nd^{16}O$.

			Collectors									
run type	config #	lines	L4	L3	L2	L1	C	H1	H2	H3	H4	integration time (s)
unspiked	1	1	*$^{134}Ba^{16}O$*	**$^{136}Ce^{16}O$**	$^{136}Ce^{17}O$	**$^{138}Ce^{16}O$**	*$^{139}La^{16}O$*	**$^{142}Ce^{16}O$**	$^{142}Ce^{17}O$	*$^{142}Ce^{18}O$*		8.39
		2	150	152	153	154	155	158	159	160		4.19
		ampli (Ω)	10^{11}	10^{11}	10^{11}	10^{11}	10^{11}	10^{11}	10^{11}	10^{11}		
unspiked	2	1	*$^{134}Ba^{16}O$*	**$^{136}Ce^{16}O$**	152.6	153.4	**$^{138}Ce^{16}O$**	154.6	$^{140}Ce^{17}O$	**$^{142}Ce^{16}O$**	*$^{142}Ce^{18}O$*	8.39
		ampli (Ω)	10^{11}	10^{12}	10^{11}	10^{11}	10^{12}	10^{11}	10^{11}	10^{11}	10^{11}	
unspiked	3	1	*$^{134}Ba^{16}O$*	**$^{136}Ce^{16}O$**	152.6	153.4	**$^{138}Ce^{16}O$**	154.6	$^{140}Ce^{17}O$	**$^{142}Ce^{16}O$**	*$^{142}Ce^{18}O$*	8.39
		ampli (Ω)	10^{13}	10^{12}	10^{13}	10^{13}	10^{12}	10^{13}	10^{11}	10^{11}	10^{11}	
unspiked	4	1	*$^{134}Ba^{16}O$*	**$^{136}Ce^{16}O$**	152.6	153.4	**$^{138}Ce^{16}O$**	154.6	**$^{140}Ce^{16}O$**	**$^{142}Ce^{16}O$**	*$^{142}Ce^{18}O$*	8.39
		ampli (Ω)	10^{13}	10^{12}	10^{13}	10^{13}	10^{12}	10^{13}	10^10	10^{11}	10^{11}	
unspiked	5	1	*$^{134}Ba^{16}O$*	**$^{136}Ce^{16}O$**	152.6	153.4	**$^{138}Ce^{16}O$**	154.6	**$^{140}Ce^{16}O$**	**$^{142}Ce^{16}O$**	*$^{142}Ce^{18}O$*	8.39
		ampli (Ω)	10^{13}	10^{12}	10^{13}	10^{13}	10^{12}	10^{13}	10^{11}	10^{11}	10^{11}	
unspiked	6	1	*$^{134}Ba^{16}O$*	**$^{136}Ce^{16}O$**	152.6	153.4	**$^{138}Ce^{16}O$**	154.6	**$^{140}Ce^{16}O$**	**$^{142}Ce^{16}O$**	*$^{142}Ce^{18}O$*	8.39
		ampli (Ω)	10^{11}	10^{11}	10^{11}	10^{11}	10^{11}	10^{11}	10^{11}	10^{11}	10^{12}	
spiked	7	1	*$^{134}Ba^{16}O$*	**$^{136}Ce^{16}O$**	152.6	153.4	**$^{138}Ce^{16}O$**	154.6	**$^{140}Ce^{16}O$**	**$^{142}Ce^{16}O$**	*$^{142}Ce^{18}O$*	8.39
		ampli (Ω)	10^{13}	10^{11}	10^{13}	10^{13}	10^{11}	10^{13}	10^{11}	10^{11}	10^12	
spiked	8	1		*^{134}Ba*	**^{136}Ce**	*^{137}Ba*	**^{138}Ce**	*^{139}La*	**^{140}Ce**	**^{142}Ce**	*^{143}Nd*	8.39
		ampli (Ω)	10^{13}	10^{11}	10^{11}	10^{11}	10^{11}	10^{11}	10^{11}	10^{11}	10^{11}	

709

710

711

712

713

714

715

716

Table 2: spikes isotopic compositions used in the theoretical calculations presented in Figure 3. See text for details.

spike	^{136}Ce	^{138}Ce	^{142}Ce
$^{136}Ce/^{140}Ce$	0.001	0.809	0.021
$^{138}Ce/^{140}Ce$	0.745	0.015	0.021
$^{142}Ce/^{140}Ce$	0.046	0.080	20.234

Table 3: Ce isotopic composition of the triple spike calibrated in this study.

	$^{136}Ce/^{140}Ce$	2 s.d.	$^{138}Ce/^{140}Ce$	2 s.d.	$^{142}Ce/^{140}Ce$	2 s.d.
LMV-Ce (n = 48)	0.00212484	0.00000008	0.0028412	0.0000001	0.125879	0.000005
Triple spike (n =21)	0.38706	0.00003	0.39570	0.00003	0.062070	0.000005

738 Table 4: Results for the radiogenic Ce isotopic composition of two solution reference materials (Ce-LMV and Ce-AMES) and two rock reference materials
739 together with data from the literature. *the uncertainties are 2 standard errors.

sample name	config #	$^{142}Ce^{16}O$ (V)	$^{138}Ce/^{142}Ce$	2 s.d.	$^{138}Ce/^{136}Ce$	2 s.d.	$\varepsilon^{138}Ce_{LMV}$	2 s.d.	$^{140}Ce/^{142}Ce$	2 s.d.	n	ref
LMV Ce	3	9.9	0.02257053	0.00000061	1.337116	0.000036	0.00	0.27	N/A	N/A	48	This study
LMV Ce	4	9.6	0.02257056	0.00000051	1.337118	0.000030	0.01	0.23	7.94397	0.00014	7	This study
LMV Ce	5	2.4	0.02257059	0.00000098	1.337120	0.000058	0.03	0.43	7.94417	0.00025	6	This study
LMV-Ce	6	2.77	0.02257062	0.00000097	1.337122	0.000057	0.04	0.43	7.94403	0.00018	10	This study
AMES-Ce	1	10.1	0.02257431	0.00000046	1.337341	0.000027	1.68	0.20	N/A	N/A	5	This study
AMES-Ce	2	9.55	0.02257426	0.00000068	1.337338	0.000040	1.66	0.30	N/A	N/A	25	This study
AMES-Ce	4	10	0.02257458	0.00000013	1.337357	0.000008	1.80	0.06	7.94416	0.00023	5	This study
AMES-Ce			0.02257497	0.00000050	1.337380	0.000030	1.97	0.22	N/A	N/A	35	Willbold 2007
AMES-Ce			0.02257468	0.00000100	1.337363	0.000059	1.84	0.44	N/A	N/A	53	Doucelance et al. 2014
AMES-Ce			0.02257320	0.00000180	1.337275	0.000107	1.18	0.80	N/A	N/A	89	Bellot et al. 2015
AMES-Ce			0.02257474	0.00000048	1.337366	0.000028	1.87	0.21	7.94333	0.00031	9	Willig and Stracke 2017
BCR-2	3	10.7	0.02256689	0.00000055	1.336901	0.000033	-1.61	0.24	N/A	N/A	5	This study
BCR-2*	4	11.2	0.02256696	0.00000020	1.336905	0.000012	-1.58	0.09	7.943620	0.000025	1	This study
BCR-2			0.02256678	0.00000066	1.336894	0.000039	-1.66	0.29	N/A	N/A	3	Doucelance et al. 2014
BCR-2			0.02256620	0.00000070	1.336860	0.000041	-1.92	0.31	N/A	N/A	4	Bellot et al. 2015
BCR-2			0.02256719	0.00000063	1.336919	0.000037	-1.48	0.28	N/A	N/A	20	Willig and Stracke 2017
BHVO-2	3	8.7	0.02256489	0.00000047	1.336782	0.000028	-2.50	0.21	N/A	N/A	2	This study
BHVO-2*	4	10	0.02256499	0.00000024	1.336788	0.000014	-2.45	0.11	7.943886	0.000032	1	This study
BHVO-2			0.02256550	0.00000154	1.336819	0.000091	-2.23	0.68	N/A	N/A	8	Doucelance et al. 2014
BHVO-2			0.02256460	0.00000170	1.336765	0.000101	-2.63	0.75	N/A	N/A	6	Bellot et al. 2015
BHVO-2			0.02256482	0.00000059	1.336778	0.000035	-2.53	0.26	N/A	N/A	24	Willig and Stracke 2017

740

741

742

743 Table 5: Results for triple spike runs performed using the Ce-LMV reference material.

sample name	run type	cup config.	spike/std	δ^{142}Ce	2 s.d.	n
LMV-Ce	oxide	5	0.20	0.008	0.099	4
LMV-Ce	oxide	5	0.33	0.023	0.052	13
LMV-Ce	oxide	5	0.50	-0.015	0.077	5
LMV-Ce	metal	6	0.33	-0.083	0.028	4

744